

# A Quasicontinuum Method for Deformations of Carbon Nanotubes

Jong Youn Park<sup>1</sup>, Young-Sam Cho<sup>2</sup>, Sung Youb Kim<sup>1</sup>, Sukky Jun<sup>3</sup> and Seyoung Im<sup>1</sup>

**Abstract:** We present a coarse-graining computation for deformations of CNTs (carbon nanotubes) via QC (quasicontinuum), particularly targeting analysis of multi-walled carbon nanotubes. Higher order triangular elements are utilized for proper interpolation of atom positions of the CNT on the basis of QC approach. The computing scheme enables one to differentiate between the fully atomistic zone and the coarse-grained zone in the framework of the multiscale computing. Several numerical examples demonstrate the effectiveness and accuracy of the present methodology.

**keyword:** Multiscale, Coarse-grained model, Carbon nanotube, Quasicontinuum method.

## 1 Introduction

There has been a keen interest in deformations of carbon nanotubes due to their various applications as mechanical components and their diverse deformation-dependent properties like electrical conductance [Tombler, Zhou, Alexseyev, Kong, Dai, Liu, Jaynathi, Tang and Wu (2000), Rueckes, Kim, Joselevich, Tseng, Cheung and Liever (2000), Liu, Jiang, Johnson and Huang (2004)]. Most straightforwardly, continuum or structural mechanics approach has been employed by many authors [Arroyo and Belytschko (2002), Jiang, Zhang, Liu, Huang, Geubelle, Gao and Hwang (2003), Gao and Li (2003), Jiang, Feng, Huang, Hwang and Wu (2004), Pantano, Parks and Boyce (2004), Liu, Jiang, Johnson and Huang (2004), Nasdala, Ernst, Lengnick and Rothert (2005)]. Among others, Arroyo and Belytschko (2002) reported a scheme for computing atomistic-based finite deformations. This provides a continuum model for curved crystalline sheets based on the exponential Cauchy-Born rule which extends the standard Cauchy-Born rule to the

case of curved crystalline structures. It was successfully applied to nonlinear mechanical deformations of multi-walled carbon nanotubes [Arroyo and Belytschko (2003)]. This method actually generalizes the *local* quasicontinuum to the case of curved crystalline structures, but does not apply to *nonlocal* domains [Tadmor, Ortiz and Phillips (1996), Shenoy, Miller, Tadmor, Phillips and Ortiz (1998), Knap and Ortiz (2001)]. Various multiscale methods have been proposed by many researchers [Broughton, Abraham, Bernstein and Kaxiras (1999), Wagner and Liu (2003), Chung, Namburu and Henz (2004), Shen and Atluri (2005)]. In multiscale problems, coarse scales are modeled by FE(finite element), or meshfree approximations [Wagner and Liu (2001), Atluri and Shen (2002)].

The effectiveness of the quasicontinuum lies in the concurrent treatment of different length scales between the local zone and the nonlocal zone for looking into the behaviors of various defects such as voids, twins, grain boundaries and dislocations [Tadmor, Miller, Phillips and Ortiz (1998), Miller, Ortiz, Phillips, Shenoy and Tadmor (1998), Rodney and Phillips (1999), Shenoy, Kukta and Phillips (2000), Knap and Ortiz (2003), Marian, Knap and Ortiz (2004)]. In actuality, this feature has made the quasicontinuum method attract a substantial amount of attention as a computational methodology for multiscale boundary value problems in solid mechanics for the past decade.

In the present paper, we report a computing scheme for deformations of carbon nanotubes in the framework of the quasicontinuum method. In a sense, it generalizes the standard quasicontinuum method to the case of a curved crystalline body, as it enables one to deal with the nonlocal quasicontinuum as well as the local quasicontinuum for curved structures. The key feature includes the use of higher order interpolation functions for accurately mapping curved geometries, and the cluster-weighted average of the interatomic potential energy for computing the force on the individual degrees of freedom. The outline of the paper is as follows. In Section 2, the computational

<sup>1</sup> Department of Mechanical Engineering, Korea Advanced Institute of Science and Technology (KAIST), Daejeon, Korea

<sup>2</sup> Department of Future Technology, Korea Institute of Machinery and Materials (KIMM), Daejeon, Korea

<sup>3</sup> Department of Mechanical and Materials Engineering, Florida International University, Miami, Florida, USA

scheme is described, and this is followed by the numerical verifications and some examples of a large-scale computation in Section 3. Finally, Section 4 concludes the paper with some remarks.

## 2 Quasicontinuum (QC) for a curved crystalline body

In this section, we discuss how to extend the standard quasicontinuum [Knap and Ortiz (2001)] for application to a crystalline body with curved geometry like carbon nanotubes. We start with a brief summary of the quasicontinuum methods.

### 2.1 Quasicontinuum for rectilinear crystalline structures

A total potential energy  $E_{total}$  of a given system is the summation of the individual potential energies  $E_i$  for all atoms in a given system :

$$E_{total} = \sum_{i=1}^N E_i \quad (1)$$

where  $N$  is the total number of the atoms in a system. Tadmor et al. (1996) and Knap and Ortiz (2001) suggested a coarse-grained approximation  $E_{total}^h$  of the energy  $E_{total}$  according to the node-based summation rule as:

$$E_{total} \approx E_{total}^h = \sum_{\alpha=1}^{N_R} w_{\alpha} E_{\alpha} \quad (2)$$

where  $N_R$  indicates a total number of the representative atoms, and  $w_{\alpha}$  and  $E_{\alpha}$  the weight function and the potential energy of the  $\alpha$ -th representative atom. The mapping from the Lagrangian variable  $\mathbf{X}_i$  to the current position  $\mathbf{x}_i$  for the  $i$ -th atom is approximated by  $\mathbf{x}_i^h$ , which is written in the form of interpolation:

$$\mathbf{x}_i^h = \sum_{\alpha=1}^{N_R} S_{\alpha}(\mathbf{X}_i) \mathbf{x}_{\alpha} \quad (3)$$

where  $S_{\alpha}(\mathbf{X}_i)$  indicates the *linear* shape function associated with the  $\alpha$ -th representative atom, and  $\mathbf{x}_{\alpha}$  the current position or the nodal value of the  $\alpha$ -th representative atom. Assuming the interpolation of the energy distribution via the same function  $S_{\alpha}(\mathbf{X}_i)$ , we have

$$E_{total}^h = \sum_{i=1}^N \sum_{\alpha=1}^{N_R} S_{\alpha}(\mathbf{X}_i) E_{\alpha} \quad (4)$$

Comparison of Eq. 2 and Eq. 4 yields the expression for the weight function

$$w_{\alpha} = \sum_{i=1}^N S_{\alpha}(\mathbf{X}_i) \quad (5)$$

Knap and Ortiz (2001) pointed out that the preceding node-based summation rules are not free from the zero energy deformation modes, which may be prevented by taking a sufficient number of sampling points. In this context, Knap and Ortiz (2001) generalized this node-based summation rule to obtain the so-called cluster-based summation rule, in which the shape function is sampled, not at nodal points, but over neighborhoods, called clusters, of the representative atoms. In this cluster-based method, each cluster plays the role of a node in the node-base rules, and so it is contemplated as a representative crystallite over which the shape function values are sampled for interpolation. A coarse-grained energy according to the cluster-based rule is given as

$$\begin{aligned} E_{total}^h &= \sum_{\beta=1}^{N_R} (w_{\beta})_{cluster} (E_{\beta})_{cluster} \\ &= \sum_{\beta=1}^{N_R} (w_{\beta})_{cluster} \left[ \sum_{i \in Cluster_{\beta}} E_i \right] \\ &= \sum_{\beta=1}^{N_R} (w_{\beta})_{cluster} \left[ \sum_{i \in Cluster_{\beta}} \sum_{\alpha=1}^{N_R} S_{\alpha}(\mathbf{X}_i) E_{\alpha} \right] \end{aligned} \quad (6)$$

where  $(w_{\beta})_{cluster}$  indicates the weight of the cluster summation rule, and the  $(E_{\beta})_{cluster}$  represents the summation of all atoms in the  $\beta$ -th cluster. From Eq. 4 and Eq. 6, it follows that

$$\sum_{\alpha=1}^{N_R} (w_{\alpha})_{cluster} \sum_{i \in Cluster_{\alpha}} S_{\beta}(\mathbf{X}_i) = w_{\beta} \quad (7)$$

where  $w_{\beta}$  is the weight function of Eq. 5 according to the node-based rule. The solution of a system of linear Eq. 7 in  $(w_{\alpha})_{cluster}$  is not that time consuming as the coefficients are given as a sparse matrix due to the localization property of the shape function  $S_{\beta}(\mathbf{X}_i)$ . Once  $(w_{\alpha})_{cluster}$  is calculated, it is straightforward to compute the internal force by differentiating the coarse-grained potential energy of Eq. 6, so that the equilibrium configuration may be obtained.

## 2.2 Extension to a curved crystalline structure

As a first step towards extending this cluster-based summation rule to the case of a curved crystalline shell structure such as a carbon nanotube, we consider the formation of a carbon nanotube from a graphene lattice sheet (see Fig. 1). We take this flat graphene sheet for the parental domain of the carbon nanotube under consideration. Limiting ourselves to the local quasicontinuum, deformations of all individual atoms obey to the Cauchy-Born hypothesis (speaking strictly the exponential Cauchy-Born rule due to the curvature of the carbon nanotube), and the locally homogeneous deformation prevails. This implies that for the local quasicontinuum the displacement of each atom is given by the deformation of the continuum-like graphene sheet, on which each atom is embedded. To be more specific, any fictitious material point which does not coincide with the atom location in the parental domain, say a point A in Fig. 1, undergoes the same mapping as the surrounding material points in the parental domain, say the points B, C, D, E, F, G in Fig. 1, as long as deformations obey to the exponential Cauchy-Born rule. This observation makes it possible to treat the graphene sheet like a continuum shell, and so any points on the graphene sheet, whether or not they coincide with the atom location, may be used as nodal points for interpolation of the current position vectors.

Let the Lagrangian variable  $\mathbf{X}_i$  denote the position vector of the  $i$ -th atom in the parental configuration or the flat graphene sheet of a carbon nanotube. Note that the current configuration cannot be written as in Eq. 3 as the linear shape function  $S_\alpha(\mathbf{X}_i)$  fails to depict curved geometries. To represent a curved shell, we need at least quadratic interpolation for the current position.

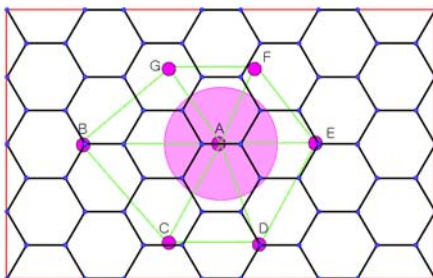


**Figure 1** : Illustration of parental domain and FE mesh on graphene (A-G are node).

The aforementioned observation now prompts us to introduce the higher order interpolations to deal with a curved geometry of carbon nanotubes. From the view of adaptability, triangular elements with the Hermite type interpolation or the quadratic or cubic Lagrange shape function are a good candidate. For convenience of modeling, the nodal points on the vertices of a triangular element are chosen such that they coincide with the atom positions on the graphene. Then the mid nodes may not fall on an atom site. However, this does not matter at all, from the argument of the preceding paragraph, as long as the local quasicontinuum is concerned. We call these nodes atomless nodes hereafter to distinguish them from the atom nodes, of which the locations coincide with atom sites on the graphene.

For clarity we denote by  $\mathbf{v}_\alpha$  the current position vector of a nodal point, which may be an atom node or an atomless node on the graphene sheet, and we represent the current configuration, which is curved in nature, by the following higher order interpolation:

$$\mathbf{x}_i^h = \sum_{\alpha=1}^{N_v} G_\alpha(\mathbf{X}_i) \mathbf{v}_\alpha \quad (8)$$

where  $N_v$  is the total number of the nodal points for displacement or position interpolation, and  $G_\alpha$  is a higher order shape function. To represent a curved geometry properly, we require  $G_\alpha$  to be a Hermite shape function, or a quadratic or cubic Lagrangian shape function. Note that the local quasicontinuum allows atomless nodal points, which occur unavoidably in applying interpolation of order higher than the linear one.

Now we consider how to sum up the interatomic potential energies over the entire domain. Suppose a mesh configuration changes from a coarse one to fine one depending on the field gradient on the local region, finally to fully atomistic or molecular mechanics model on the nonlocal zone. In the nonlocal region, the connection of the locations of the neighboring atoms leads to linear triangular elements. Accordingly, the linear interpolation is a natural choice for the energy interpolation from the view of consistent refinement from a coarse to fine mesh. In addition, for the higher order elements, it is troublesome to handle the atomless nodes, which are inevitable in the higher order interpolation of the energy. It is awkward to link a potential energy to an atomless node for interpolation, though atomless nodes are allowable in interpolating the position vectors due to the locally homogeneous

deformations. Conclusively, we choose the linear shape function (3) to interpolate the potential energy

$$E_i^h = \sum_{\alpha=1}^{N_R} S_{\alpha}(\mathbf{X}_i) E_{\alpha} \quad (9)$$

Then, the total potential energy based on the cluster-based summation rule is given by Eq. 6 with the weight  $(w_{\beta})_{cluster}$  being given by Eq. 7. Noting that the cluster potential energy  $(E_{\beta})_{cluster}$  is written as

$$(E_{\beta})_{cluster} = \sum_{i \in Cluster_{\beta}} E_i \quad (10)$$

and that each atom's contribution  $E_i$  depends on the current configuration, given by Eq. 8, we see that the resulting expression for the potential energy depends on the variables  $\mathbf{v}_{\alpha}$  ( $\alpha = 1 \sim N_v$ ).

The equilibrium equation is obtained by differentiating or minimizing, with respect to  $\mathbf{v}_{\alpha}$ , the total potential energy. For a multi-walled carbon nanotube, the total potential energy comprises the chemical bonding potential energy on each plane of the nanotube sheets and the non-bonding potential energy between two neighboring walls of the multi-walled carbon nanotube. The potential energy from the applied traction should be added to these if there is a traction imposed on the boundary.

Most straightforward implementation of the aforementioned scheme is as follows. Firstly, we construct a quasicontinuum mesh composed of higher order triangular elements for the position vector interpolation, given by Eq. 8, with the vertex nodes being made atom nodes. Next, we remove all mid nodes in these higher order elements, and use the resulting linear triangular element for the potential energy representation Eq. 9. Minimizing the total potential energy or taking its gradient with respect to the current position vector  $\mathbf{v}_{\alpha}$ , we can obtain force equilibrium equation.

### 3 Numerical examples

In this section, we apply the scheme discussed in the previous section for various deformations of carbon nanotubes to check the accuracy. Firstly, we test the cases of simple deformations, such as bending and torsion, for which comparison is made with the results from the fully atomistic simulation or the molecular mechanics simulation.

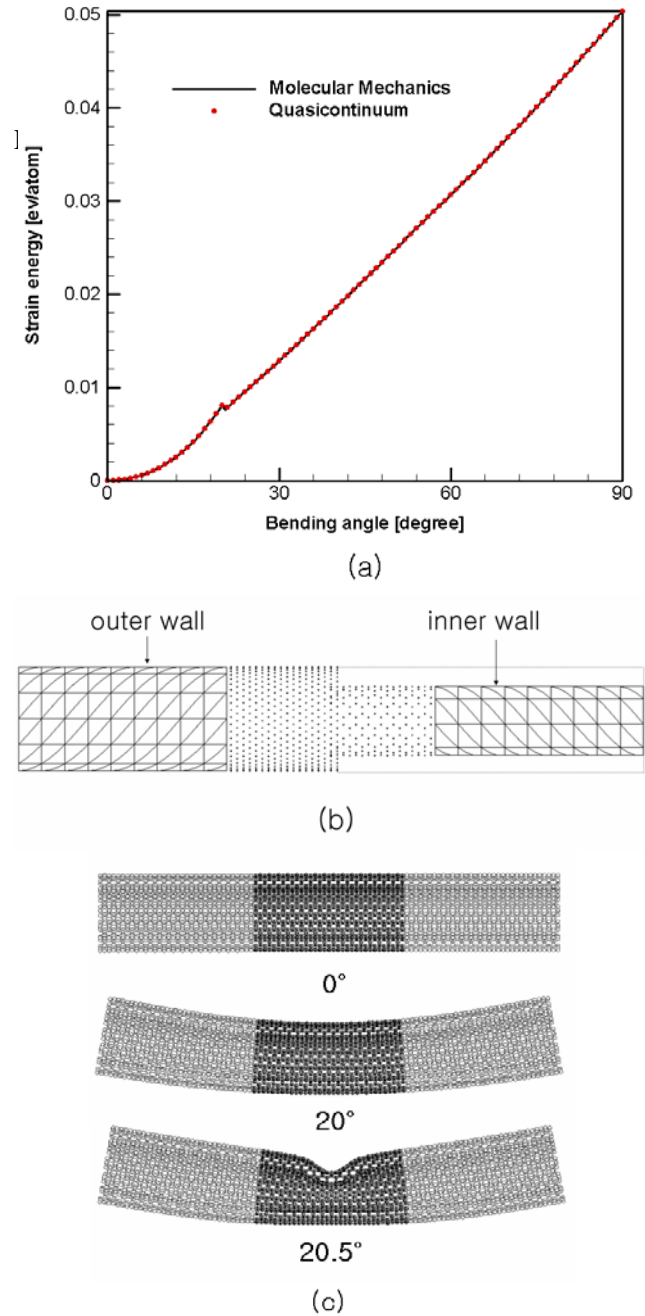


**Figure 2** : Bending simulation for DWCNT (a) strain energy per atom under bending load (Model 4), (b) QC models for outer tube and inner tube (Model 4) and (c) cross section of deformed configuration at each bending angle (Model 4). The black indicates fully atomistic zone and the gray QC zone.

We choose Tersoff-Brenner potential [Tersoff (1988), Brenner (1990)] for the interatomic bonded interac-

**Table 1** : The total number of degrees of freedom and percentile errors in strain energy at each bending angles for four considered QC models. The angles described at the first column mean the bending angles.

	Model 1	Model 2	Model 3	Model 4
DOF	10080	12870	13950	15030
Error at 45 °	1.72	1.37	0.58	0.05
Error at 90 °	2.97	2.35	0.97	0.08

**Table 2** : The total number of degrees of freedom and percentile errors in strain energy for four considered QC models which have uniform FE mesh. The angles described at the first column mean the twisting angles.

	Model 1	Model 2	Model 3	Model 4
DOF	6372	8001	10008	11988
Error at 49 °	3.63	3.64	2.27	0.08
Error at 77 °	5.34	4.92	3.11	0.13
Error at 120 °	7.51	6.27	3.78	0.17
Error at 240 °	17.55	13.30	8.08	0.48
Error at 360 °	33.42	25.59	16.87	1.06

tion on the individual surface of carbon nanotubes, and Lennard-Johns type function [Girifalco, Hodak and Lee (2000)] to represent the nonbonded interaction between two neighboring walls. The role of this nonbonded potential is very important when rippling or buckling occurs such that the tube wall may come into van der Waal's contact [Arroyo and Belytschko (2004)]. For minimization, LBFGS (Limited-memory BFGS) [Nocedal (1980), Liu and Nocedal (1989)], which is known as an efficient quasi-Newton method, is adopted.

### 3.1 Bending of a double-walled CNT (DWCNT)

Our first numerical example is the bending of a 12.6 nm long DWCNT, in which van der Waal's interactions are critical. The chiralities are (10,10) for the inner layer and (15,15) for the outer layer, and the bending is imposed by rotating each end in the opposite directions. The number of degrees of freedom in QC models ranges from 10080 (Model 1) to 15030 (Model 4) while the total number of degrees of freedom in the fully atomistic or molecular mechanics (MM) model is 15150 (See Table 1 for detail). Fig. 2(a) and 2(c) show the strain energies versus bending angle, and deformed configurations for three bending angles 0°, 20° and 20.5° for the QC model like Fig. 2(b) with the number of degrees of freedom 15030. FE mesh and atomistic zone of the half model for inner and outer tubes are given in Fig. 2(b).

In Fig. 2(c), the black indicates the fully atomistic zone

wherein every individual atom is included while the gray the QC zone wherein the finite element interpolation is taken. Unless mentioned otherwise, all figures are colored in this way. A kink occurs at the center when the bending angle reaches 20.5°, which is indicated by an abrupt protrusion on the energy curve in Fig. 2(a). The percentile errors of the total energy relative to the result from the MM model are tabulated for each of the QC models in Table 1. In case of error in deformation, the QC result atomic distance between the two walls at the center after kink (at bending angle 20.5°) differs only 0.28% from the MM result, even for the coarsest model, which is negligibly small just like the errors in energy. As far as interpolation order is concerned, it turns out that the cubic Hermite shape function and the 3rd order Lagrange shape function lead to the same degree of accuracy in the numerical results.

### 3.2 Torsion of a single-walled CNT (SWCNT)

In this section, we take a torsion example for 25 nm long (10,10) armchair CNT and it is twisted by imposing rotations in the opposite directions at each end. The maximum angle of twist is 360°, which amounts to torsion of 1.433[degree/Å]. Four different models depending on the refinement have a total number of degrees of freedom 6372, 8001, 10008, 11988, respectively, while MM model has 12060. Note that the maximum number of degrees of freedom of the present model does not exceed

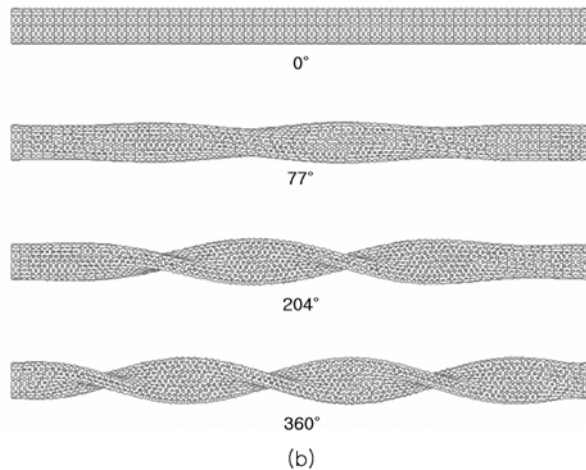
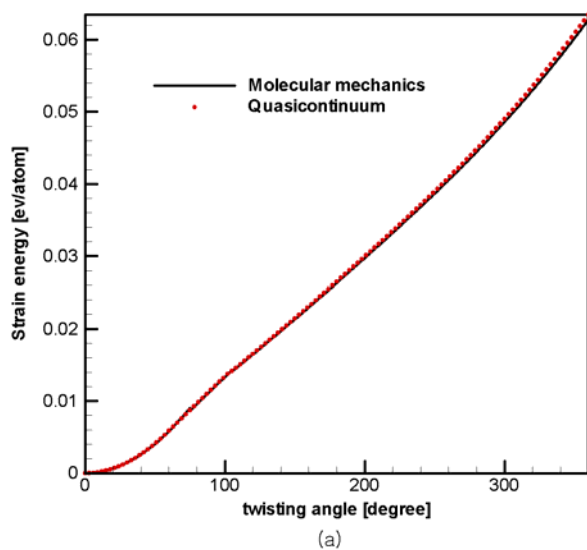


**Figure 3** : Torsional simulation for SWCNT (a) Strain energy per atom under twisting load (Model 4) and (b) deformed configuration at each twisting angle (Model 4).

the number of degrees of freedom of the fully atomistic model.

Fig. 3(a) shows the strain energy versus twisting angle, and it shows that the total strain energy is in good agreement when compared with the result from MM simulation. Fig. 3(b) shows the deformed configurations corresponding to four values of the twist angles  $0^\circ$ ,  $77^\circ$ ,  $204^\circ$ ,  $360^\circ$ . The onset of the inhomogeneous deformation occurs at the twist angle of  $49^\circ$ , and it propagates into other area as deformation proceeds. The two walls begin to get in contact with each other at the twist angle of  $72^\circ$ . A noticeable difference from the bending case is that the location of the onset of the inhomogeneous de-

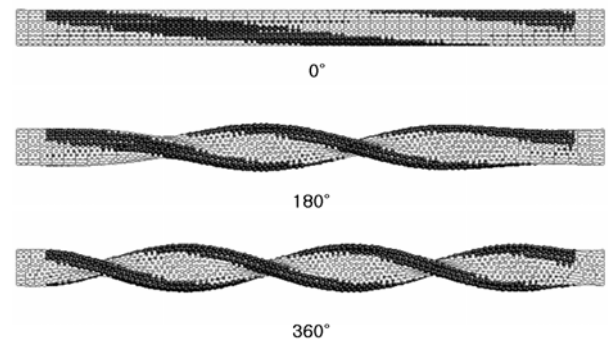


**Figure 4** : Deformed configuration in QC model which retains refined mesh along the helical zone of deformation localization (Model 4). The black indicates fully atomistic zone and the gray QC zone.

formation is not predictable in torsion, while it always occurs at the center in bending.

If the refinement is not enough to capture the localized inhomogeneous deformation, the accuracy of QC deteriorates. This is why the results from QC deviate greatly from MM result, as shown in Table 2. Therefore, for more accurate analysis of twisting, we may need a scheme of adaptive meshing to control the mesh refinement according to the severity of deformations. We do not try this exactly, but we investigate a possible efficacy of adaptive meshing by constructing the mesh in the following way. From the preceding analysis we pinpoint the zone of localization, which is along the helical direction. Initial mesh is refined along this localization zone, as shown in Fig. 4. Four different models depending on the refinement have a total number of degrees of freedom 5850, 6219, 7587, 8208, respectively. Although these QC models have a total number of degrees of freedom near the number of degree of freedom for the previous coarse models which have uniform FE mesh, errors in energy remarkably decrease as shown in Table 3.

### 3.3 Bending of a perfect and a defective 5-walled CNT

In this section, we simulate bending of 5-walled carbon nanotubes with their length 28.13 nm. The chiralities from the inner wall to the outer wall are (9,0), (18,0), (27,0), (36,0), (45,0). We consider three cases. The first is a perfect 5-walled CNT (see Fig. 5(a)), and the second is the case wherein the inner three walls are dissected into two at the center and each of the end surfaces generated from the cut is capped with the half of fullerene. The

**Table 3** : The total number of degrees of freedom and percentile errors in strain energy for four considered QC models which retain refined mesh along the helical zone of deformation localization. The angles described at the first column mean the twisting angles.

	Model 1	Model 2	Model 3	Model 4
DOF	5850	6219	7587	8208
Error at 49 °	1.92	1.90	1.73	1.64
Error at 77 °	3.35	3.37	2.49	2.38
Error at 120 °	2.91	2.87	2.03	1.93
Error at 240 °	3.95	3.83	2.42	2.28
Error at 360 °	6.62	6.43	4.82	4.43

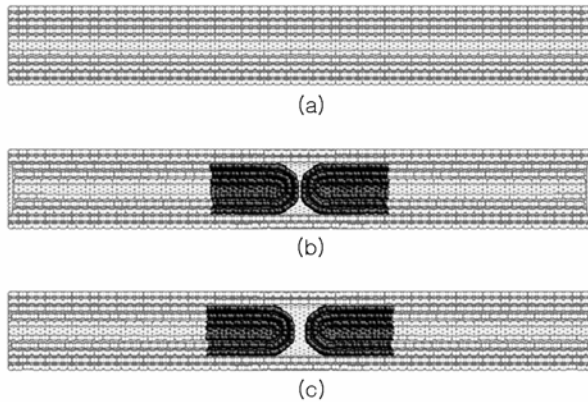


**Figure 5** : Cross sectional views of QC models for bending 5WCNTs (a) perfect walls and (b,c) inner three walls are capped with half the fullerene. The black indicates fully atomistic zone and gray QC zone.

gap between the fullerenes at the center is 3.4 Å (see Fig. 5(b)). The third is the same as the second case except that the distance between the two fullerene caps is now 7.6 Å (see Fig. 5(c)). The second and the third examples are the so-called bamboo structure, experimentally observed by Cumings and Zettl (2000). Here we take a smaller diameter than reported by Cumings and Zettl (2000). The total numbers of degrees of freedom for each case is tabulated in Table 4 together with those of the present quasicon- tinuum models. Bending is imposed on each end of the carbon nanotubes by prescribing rotation in the opposite directions up to 45 ° of the total bending angle.

In the first model, smooth bending is progressed until two kinks take place around the center at the bending angle 14.4 °, and they take the configuration as shown in Fig. 6(a) at the bending angle 15.3 °. Next a pair of the

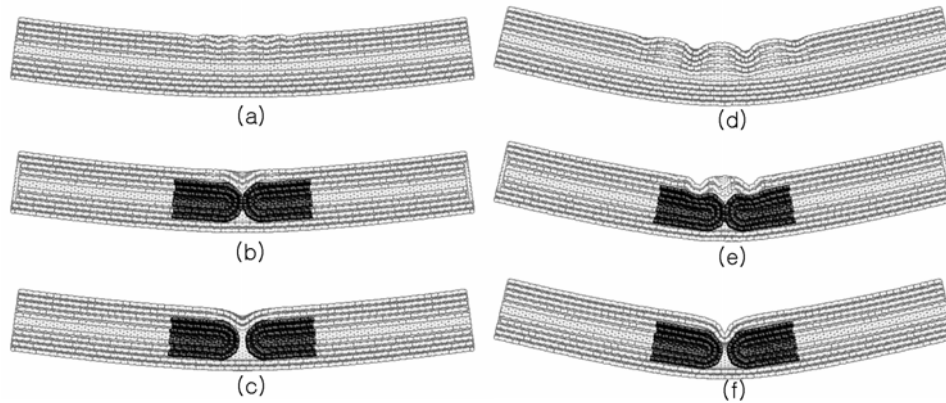
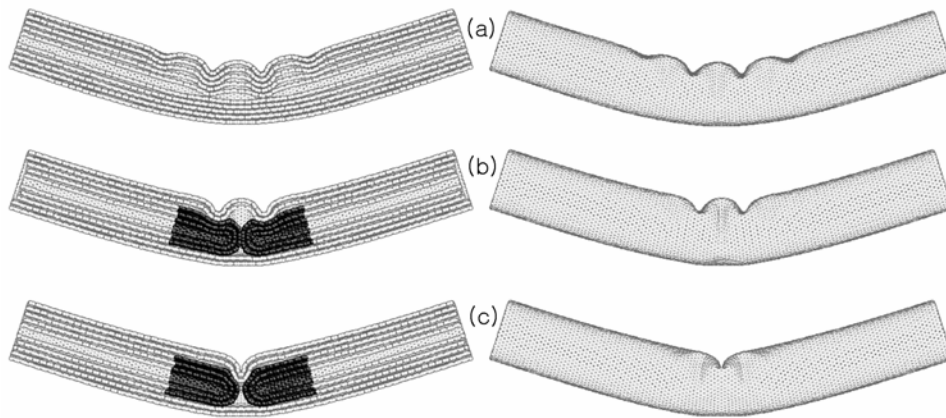
buckles or ripples occur between two neighboring kinks (see Fig. 6(d)) at the bending angle 27.0 °. This is in contrast with the result from the reference [Arroyo and Belytschko (2004)], which reports a single initial kink. The reference [Arroyo and Belytschko (2004)] simulates a case of geometry similar to the structural deformation observed by Iijima et al. (1996), and the diameter of this nanotube is about two times larger than the one in the present example.

In the second example, which models the bamboo structure, a single kink occurs on the center at the bending angle 7.2 °, and this kink grows into the space (see Fig. 6(b)) between the two caps of the inner walls until rippling or wrinkling arises due to the increasing repulsive steric force between the second outer wall and the caps' surface at the bending angle 19.8 °. At 27.0 ° of the bending angle, it takes the deformed configuration as shown in Fig. 6(e). In the third model, one kink occurs and grows into the gap space between the two caps, as in the second model (see Fig. 6(c) and (f)). However, due to the larger gap between the two caps than in the second model, the kink continues to grow into the gap space (compare Fig. 7(b) and 7(c)) until it is hampered by a large steric force from the cap surface. As deformation proceeds further, the additional kinks and rippling take place.

The three-dimensional perspective view of the deformed configurations for each of the three models are shown in Fig. 8, where each structure shows its own deformation pattern depending on its internal structure, that is, a uniform structure and bamboo structures with different cap distances. As illustrated in the examples, nonbonded interaction plays an important role in the local deformations, particularly when deformation mode like kinking or rippling occurs.

**Table 4** : The total number of degrees of freedom for MM and QC model in bending simulation for 5WCNTs.

	MM Model 1 (perfect)	QC Model 1 (perfect)	MM Model 2, 3 (capped)	QC Model 2, 3 (capped)
DOF	105300	65340	103500	69588

**Figure 6** : Cross section of equilibrium configuration for three considered QC models at (a-c) bending angle  $15.3^\circ$  and (d-f) bending angle  $27.0^\circ$ . The black indicates fully atomistic zone and gray QC zone.**Figure 7** : Cross section (left) and front view (right) of equilibrium configuration for three considered QC models at bending angle  $36^\circ$ . The black indicates fully atomistic zone and gray QC zone.

### 3.4 Cluster radius study for nonlocal formulation of QC

In this subsection, we take an example of bending to examine the influence of the size of the cluster radius for calculating the potential energy. For large scale simulation (in next subsection), it is not efficient to calculate energy of all of atoms. Therefore, cluster-based summation for energy is adopted. A 43.36nm long (60,0) SWCNT is used for this simulation. One quarter of the entire domain around the center is chosen for the fully atomistic zone

as deformation is localized around the center in bending. The total number of atoms is 24000, which amounts to the total number of degrees of freedom 72000. The total number of degrees of freedom in QC model is 28656, which is about 40% of MM model. The mesh configuration of QC model and the fully atomistic zone are shown in Fig. 9(a). Bending is applied in the same way as in the preceding subsection, and the imposed bending angle ranges from  $0^\circ$  to  $25^\circ$ .

If the cluster radius is greater than  $14.1 \text{ \AA}$ , which is ap-

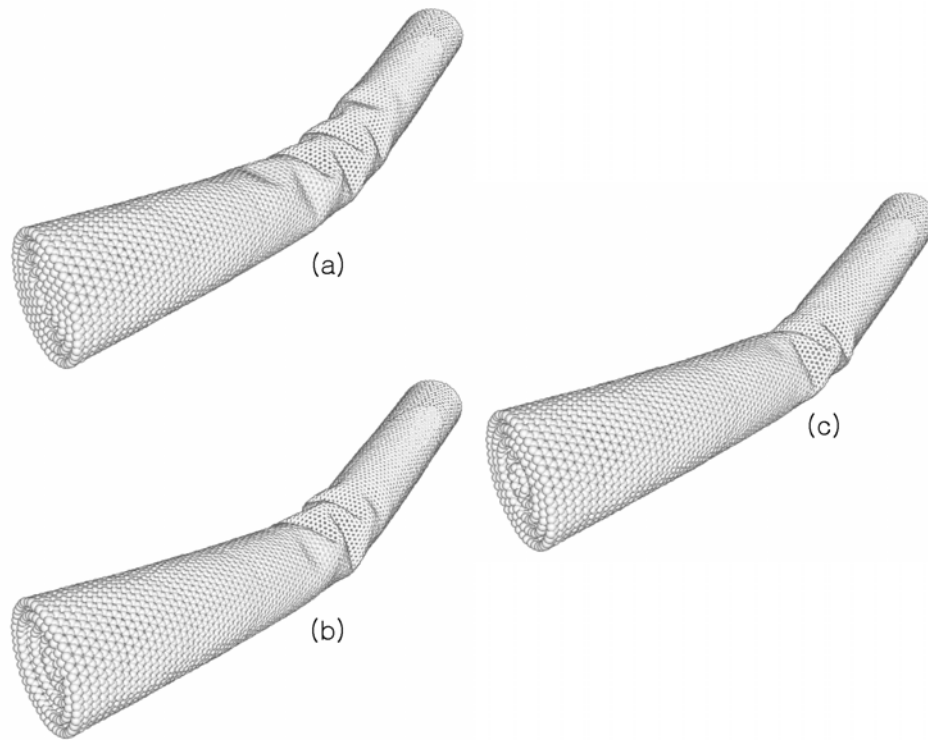


**Figure 8** : Perspective view of equilibrium configuration for three considered QC models at bending angle  $36^\circ$  (a) perfect 5WCNT, inner three walls are capped with half the fullerene (b) fullerene gab is  $3.5 \text{ \AA}$  and (c)  $7.6 \text{ \AA}$ .

proximately 10 times the bond length of graphene ( $1.45 \text{ \AA}$ ), the boundaries of any two neighboring clusters meet with each other over the entire domain. The size of the cluster radius varies from 6 times to 10 times the graphene bond-length, and the energy and deformation are calculated for each of the different cluster radii. Fig. 9(b) shows the energy versus the bending angle, and the maximum error at the bending angle  $25^\circ$  is about 6%. This error looks not small, but in terms of the deformed configuration, QC results are very close to MM result, as shown in Fig. 9(c), which depicts the comparison of the deformed configurations at the bending angle  $25^\circ$  between the three calculations: one from QC with the cluster radius  $8.7 \text{ \AA}$  (6 times the bond length), another from QC with the cluster radius  $14.1 \text{ \AA}$  (10 times the bond length) and the other from MM. The computing time for QC model with the cluster radius  $8.7 \text{ \AA}$  is only 28 % of that of the MM model.

### 3.5 Bending of a 15-walled CNT

In this section, we perform a large scale simulation in order to demonstrate superiority of proposed coarse-grained scheme. A 15-walled carbon nanotube with its

length  $62.54 \text{ nm}$  and diameter  $11.08 \text{ nm}$  is used for bending simulation (see Fig. 10(a) and Fig. 10(b)). In this simulation, entire domain is modeled by FE mesh for QC zone like Fig. 10(a). The chiralities from the inner wall to the outer wall are  $(10,10)$ ,  $(15,15)$ , ...,  $(80,80)$ . This MWCNT containing 673650 atoms has over two million degrees of freedom. QC model used in this simulation consists of 253908 degrees of freedom which is less than 13% of fully atomistic calculations. In this system, entire domain is subdivided by QC zone. As cluster radius is  $4.5 \text{ \AA}$ , it is about 60% of maximum radius. Bending is applied in the same way as in the preceding subsection, and the imposed bending angle ranges from  $0^\circ$  to  $30^\circ$ . At final stage for bending angle, this result reveals three-dimensional picture of buckles. Even though the system considered is smaller than size observed in reference [Poncharal, Wang, Ugarte and de Heer (1999)], this deformation agrees very well with rippling structure reported in experiment [Poncharal, Wang, Ugarte and de Heer (1999)] and in simulation [Arroyo and Belytschko (2004)]. Ripples shown in Fig. 10(c) are built up by sequences of simple two buckles on top and two tilted buckles on side (see Fig. 10(d) and 10(e)).

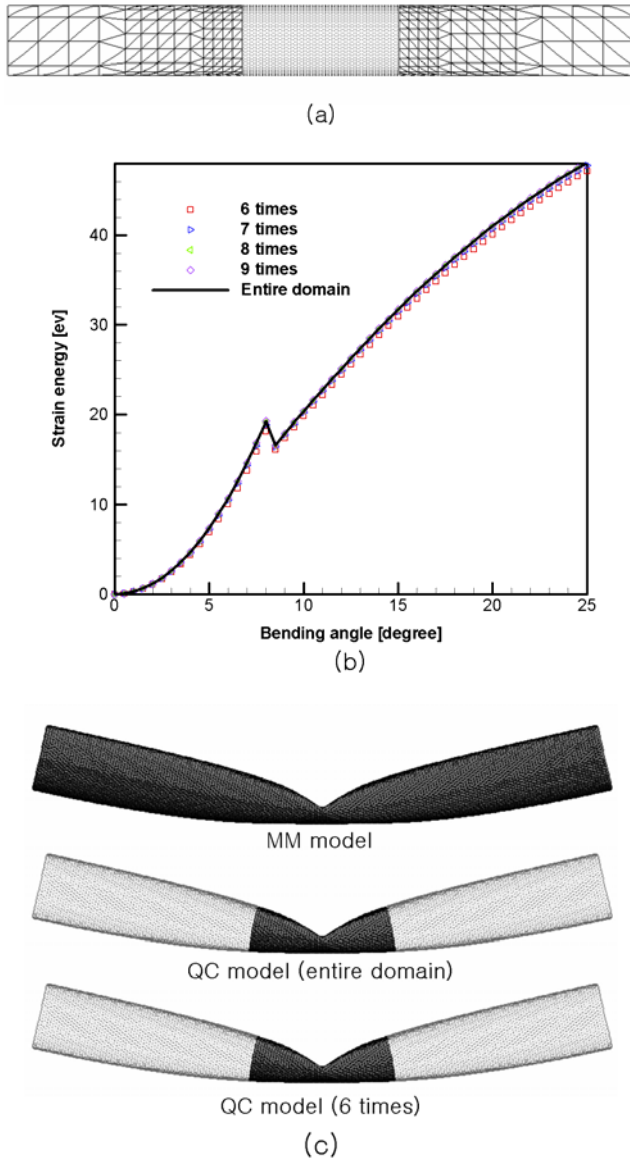


**Figure 9 :** (a) QC model for study of cluster radius, (b) strain energy curve during bending simulation with different cluster radii and (c) deformed configurations for fully atomistic simulation and for QC simulations at bending angle  $25^\circ$ .

#### 4 Conclusion

In this paper, we propose a simple method of extending the conventional QC to the case of a curved crystalline body like CNTs. We have introduced a concept of atomless degrees of freedom, which makes it possible to employ the higher order interpolations for the position and

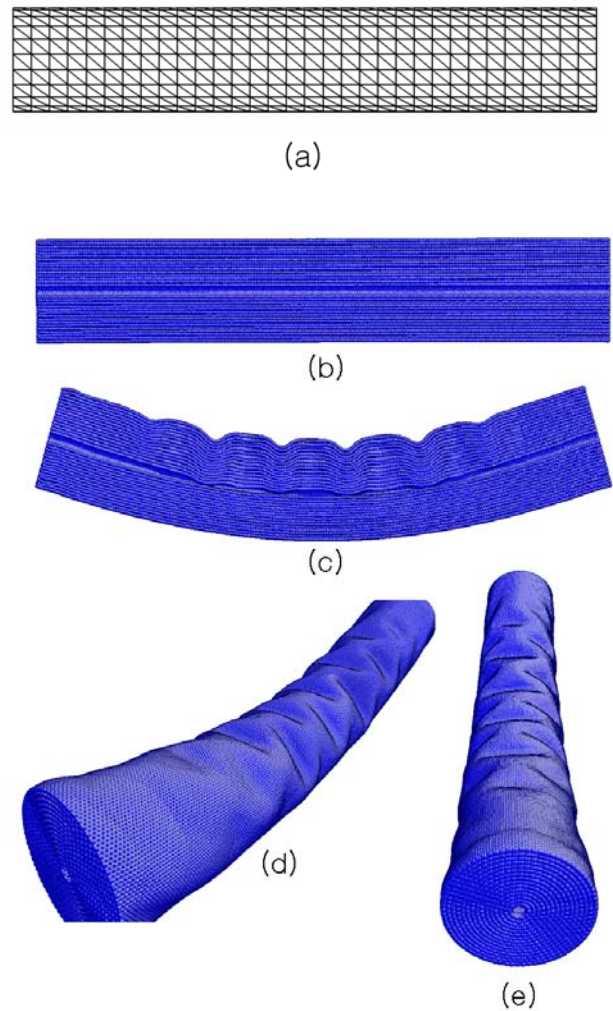


**Figure 10 :** Bending simulation for 15-walled (a) FE mesh of 15th wall in QC model, (b) a cross section of initial configuration, (c-e) a cross section and perspective views of equilibrium configuration at the bending angle  $30^\circ$ .

displacement vectors in the cluster based QC. This enables us to treat nonlocal zones as well as local zones in deformations of curved crystalline sheets. Various numerical examples demonstrate the effectiveness and the limitation of the present schemes.

**Acknowledgement:** This work was supported by the Ministry of Science and Technology of Korea through the National R&D Project for Nano Science and Technology (Grant no. M1-0213-04-0003). The authors would like to acknowledge the support from KISTI (Korea Insti-

tute of Science and Technology Information) under 'the 6th Strategic Supercomputing Applications Support Program'. The use of the computing system of the Supercomputing Center is also greatly appreciated.

## References

- Arroyo, M.; Belytschko, T.** (2002): An atomistic-based finite deformation membrane of single layer crystalline films. *Journal of the Mechanics and Physics of Solids* 50: 1941-1977.
- Arroyo, M.; Belytschko, T.** (2003): Nonlinear mechanical response and rippling of thick multiwalled carbon nanotubes. *Physical Review Letters* 91: 215505-215508.
- Arroyo, M.; Belytschko, T.** (2004): Finite element methods for the non-linear mechanics of crystalline sheets and nanotubes. *International Journal for Numerical Methods in Engineering* 59: 419-456.
- Atluri, S. N.; Shen, S.** (2002): The meshless local Petrove-Galerkin(MLPG) approaches for weakly-singular traction & displacement boundary intergral equations. *CMES: Computer Modeling in Engineering & Sciences* 3 (1): 11-52
- Brenner, D. W.** (1990): Empirical potential for hydrocarbons for use in simulating the chemical vapor deposition of diamond films. *Physical Review B* 42: 9458-9471.
- Broughton, Q. J.; Abraham, F. F.; Bernstein, N.; Kaxiras, E.** (1999): Concurrent coupling of length scales: Methodology and application. *Physical Review B* 60: 2391-2403.
- Chung, P. W.; Namburu, R. R.; Henz, B. J.** (2004): A lattice statics based tangent stiffness finite element method. *CMES: Computer Modeling in Engineering & Sciences* 5: 45-62.
- Cumings, J.; Zettl, A.** (2000): Low-Friction Nanoscale linear bearing realized from multiwall carbon nanotubes. *Science* 289: 602-604.
- Gao, X. -L.; Li, K.** (2003): Finite deformation continuum model for single-walled carbon nanotubes. *International Journal of Solids and Structures* 40: 7329-7337.
- Girifalco, L. A.; Hodak, M.; Lee, R. S.** (2000): Carbon nanotubes, buckyballs, ropes and a universal graphitic potential. *Physical Review B* 62: 13104-13110.
- Iijima, S.; Brabec, C.; Maiti, A.; Bernholc, J.** (1996): Structural flexibility of carbon nanotubes. *Journal of Chemical Physics* 104: 2089-2092.
- Jiang, H.; Zhang, P.; Liu, B.; Huang, Y.; Geubelle, P. H.; Gao, H.; Hwang, K. C.** (2003): The effect of nanotube radius on the constitutive model for carbon nanotubes. *Computational Materials Science* 28: 429-442.
- Jiang, H.; Feng, X. -O.; Huang, Y.; Hwang, K. C.; Wu, P. D.** (2004): Defection nucleation in carbon nanotubes under tension and torsions: Stone-Wales transformation. *Computer Methods in Applied Mechanics and Engineering* 193: 3419-3429.
- Knap, J.; Ortiz, M.** (2001): An analysis of the quasicontinuum method. *Journal of the Mechanics and Physics of Solids* 49: 1899-1923.
- Knap, J.; Ortiz, M.** (2003): Effect of Indenter-Radius Size on Au(001) Nanoindentation. *Physical Review Letters* 90: 216102-216105.
- Liu, B.; Jiang, H.; Johnson, H. T.; Huang, Y.** (2004): The influence of mechanical deformation on the electrical properties of single wall carbon nanotubes. *Journal of the Mechanics and Physics of Solids* 52: 1-26.
- Liu, D. C.; Nocedal, J.** (1989): On the limited memory BFGS method for large-scale optimization. *Mathematical Programming* 45: 503-528.
- Marian, J.; Knap, J.; Ortiz, M.** (2004): Nanovoid Cavitation by Dislocation Emission in Aluminum. *Physical Review Letters* 93: 165503-165506.
- Miller, R.; Ortiz, M.; Phillips, R.; Shenoy, V.; Tadmor, E. B.** (1998): Quasicontinuum models of fracture and plasticity. *Engineering Fracture Mechanics* 61: 427-444.
- Nasdala, L.; Ernst, G.; Lengnick, M.; Rothert, H.** (2005): Finite element analysis of carbon nanotubes with Stone-Wales defects. *CMES: Computer Modeling in Engineering & Sciences* 7 (3): 293-304
- Nocedal J.** (1980): Updating quasi-Newton matrices with limited storage. *Mathematics of Computation* 24: 773-782.
- Pantano, A.; Parks, D. M.; Boyce, M. C.** (2004): Mechanics of deformation of single- and multi-wall carbon nanotubes. *Journal of the Mechanics and Physics of Solids* 52: 789-821.
- Poncharal, P.; Wang, Z. L.; Ugarte, D.; de Heer, W. A.** (1999): Electrostatic deflections and electromechanical resonances of carbon nanotubes. *Science* 283: 1513-1516.
- Rodney, D.; Phillips, R.** (1999): Structure and strength of dislocation junctions: An atomic level analysis. *Physical Review Letters* 82: 1704-1707.

**Rueckes, T.; Kim, K.; Joselevich, E.; Tseng, G. Y.; Cheung, C. L.; Lieber, C. M.** (2000): Reversible, bistable carbon nanotube devices for molecular computing. *Science* 289: 94-97.

**Shen, S.; Atluri, S. N.** (2005): A tangent stiffness MLPG method for atom/continuum multiscale simulation. *CMES: Computer Modeling in Engineering & Sciences* 7: 49-67.

**Shenoy, V. B.; Miller, R.; Tadmor, E. B.; Phillips, R.; Ortiz, M.** (1998): An adaptive finite element approach to atomic-scale mechanics—the quasicontinuum method. *Journal of the Mechanics and Physics of Solids* 47: 661-642.

**Shenoy, V. B.; Kukta, R. V.; Phillips, R.** (2000): Mesoscopic analysis of structure and strength of dislocation junctions in fcc metals. *Physical Review Letters* 84: 1491-1494.

**Tadmor, E. B.; Ortiz, M.; Phillips, R.** (1996): Quasicontinuum analysis of defects in solids. *Philosophical Magazine A* 73: 1529-1563.

**Tadmor, E. B.; Miller, R.; Phillips, R.; Ortiz, M.** (1998): Nanoindentation and incipient plasticity. *Journal of Materials Research* 14: 2233-2250.

**Tersoff, J.** (1988): Empirical interatomic potential for carbon, with applications to amorphous carbon. *Physical Review Letters* 61: 2879-2882.

**Tomblar, T. W.; Zhou, C.; Alexseyev, L.; Kong, J.; Dai, H.; Liu, L.; Jayanthi, C. S.; Tang, M.; Wu, S.** (2000): Reversible electromechanical characteristics of carbon nanotubes under local probe manipulation. *Nature* 405: 769-772.

**Wagner, G. J.; Liu, W. K.** (2001): Hierarchical enrichment for bridging scales and mesh-free boundary conditions. *International Journal for Numerical Methods in Engineering* 50: 507-524.

**Wagner, G. J.; Liu, W. K.** (2003): Coupling of atomistic and continuum simulations using a bridging scale decomposition. *Journal of Computational Physics* 190: 249-274.